chemengineering

MDPI

Article

Invertase Immobilization on Magnetite Nanoparticles for Efficient Fructooligosaccharide Generation: A Comprehensive Kinetic Analysis and Reactor Design Strategy

David Polanía Melo [1], Andrés Hernández Bravo [1], Juan C. Cruz [1,2,*] and Luis H. Reyes [1,2,*]

[1] Product and Process Design Research Group (GDPP), Department of Chemical and Food Engineering, Universidad de Los Andes, Bogotá 111711, Colombia
[2] Biomedical Engineering Research Group (GIB), Department of Biomedical Engineering, Universidad de Los Andes, Bogotá 111711, Colombia
* Correspondence: jc.cruz@uniandes.edu.co (J.C.C.); lh.reyes@uniandes.edu.co (L.H.R.); Tel.: +57-61-3394949 (ext. 1702) (L.H.R.)

Abstract: This study investigated the effectiveness of immobilizing *Saccharomyces cerevisiae* invertase (SInv) on magnetite nanoparticles to produce fructooligosaccharides (FOSs). Based on the existing literature and accompanied by parameter estimation, a modified kinetic model was employed to represent the kinetics of sucrose hydrolysis and transfructosylation using SInv immobilized on magnetite nanoparticle surfaces. This model was utilized to simulate the performance of batch reactors for both free and immobilized enzymes. The maximum FOS concentration for the free enzyme was determined to be 123.1 mM, while the immobilized case achieved a slightly higher concentration of 125.4 mM. Furthermore, a continuous stirred-tank reactor (CSTR) model was developed for the immobilized enzyme, resulting in a maximum FOS concentration of 73.96 mM at the reactor's outlet and a dilution rate of 14.2 h^{-1}. To examine the impact of glucose inhibition on FOS production, a glucose oxidase reaction mechanism was integrated into the fitted immobilized theoretical model. In a batch reactor, the reduction or elimination of glucose in the reactive media led to a 2.1% increase in FOS production. Immobilizing the biocatalyst enhanced the overall performance of SInv. This enzyme immobilization approach also holds the potential for coupling glucose oxidase onto functionalized nanoparticles to minimize glucose inhibition, thereby improving FOS synthesis and facilitating optimal enzyme recovery and reuse.

Keywords: fructooligosaccharides; invertase; nanoparticles; immobilization; modeling; glucose inhibition; batch modeling; CSTR modeling

check for updates

Citation: Polanía Melo, D.; Hernández Bravo, A.; Cruz, J.C.; Reyes, L.H. Invertase Immobilization on Magnetite Nanoparticles for Efficient Fructooligosaccharide Generation: A Comprehensive Kinetic Analysis and Reactor Design Strategy. *ChemEngineering* **2023**, *7*, 55. https://doi.org/10.3390/chemengineering7030055

Academic Editor: Vasile Lavric

Received: 6 April 2023
Revised: 8 May 2023
Accepted: 9 May 2023
Published: 12 June 2023

Copyright: © 2023 by the authors. Licensee MDPI, Basel, Switzerland. This article is an open access article distributed under the terms and conditions of the Creative Commons Attribution (CC BY) license (https://creativecommons.org/licenses/by/4.0/).

1. Introduction

Fructooligosaccharides (FOSs) are short-chained fructans (fructose-based polymers) that possess advantageous physicochemical and physiological properties due to the presence of β-glycosidic bonds. These properties make FOSs a highly desired functional food ingredient [1–3], offering a low-calorie alternative with a sweetness level comparable to that of sucrose and promoting benefit-specific microbial growth due to their resistance to human enzymatic hydrolysis (i.e., prebiotic properties) [2]. Consequently, FOSs are becoming increasingly desirable for designing marketable products, and it is crucial to develop cost-effective production techniques to meet the growing demand for them [1].

FOS synthesis can occur via two mechanisms: inulin degradation by endoinulinase-catalyzed hydrolysis and sucrose degradation and modification by hydrolytic and transfructosylating enzymatic catalysis [3]. Invertase, a key enzyme for sucrose hydrolysis into glucose and fructose and sucrose transfructosylation into FOS, has attracted significant interest over the years. Consequently, the reaction kinetics, operating parameters, and transfructosylation activity of invertase have been extensively investigated [1]. Invertase,

also known as β-fructosidase, belongs to the glycosyl hydrolase family GH32, and its activity depends on the substrate concentration, pH, temperature, and enzyme purity and origin. Khandekar et al. report that the optimal synthesis of FOS using purified invertase from *S. cerevisiae* occurs at 40 °C and a pH of 5.5 [1]. However, Kulshrestha et al. report that invertase's maximum enzymatic activity occurs at 50 °C and a pH of 4.5 [4]. Veana et al. even report invertase having its maximum enzymatic activity between 25 and 35 °C and at a pH between 4.5 and 5 [5]. Invertase enzymatic activity is inhibited by compounds such as fructose, glucose, and heavy metal cations [1,6,7]. Invertases from molds, yeasts, and fungi tend to preferentially utilize sucrose as a substrate [5].

Invertases have dual hydrolysis and transfructosylation activities depending on the substrate's concentration. Hydrolysis occurs at low sucrose concentrations (about 10%), whereas their transferring activity occurs at higher concentrations (20–85%). Sucrose hydrolysis yields equimolar fructose and glucose (inverted sugars) as primary products. The transfructosylation reaction catalyzed by invertase involves the addition of fructofuranosyl residues to sucrose to produce FOSs, such as 1-kestose, nystose, and fructofuranosylnystose, among others [5,8]. A study by Khandekar et al. demonstrated that the maximum FOS yield (10%) was achieved at an initial substrate concentration of approximately 525 g/L [1]. They also determined that the optimal enzyme concentration for maximum FOS production was around 2 U/mL. Beyond this concentration, the maximum FOS yield can be reached in shorter reaction times; however, this may result in a decline in the FOS concentration due to the dominance of hydrolysis over synthesis [1].

A significant challenge for the industrial application of enzymes, including invertase, is maintaining their stability and activity under controlled temperature, pH, and substrate concentrations in bioreactors [9]. Maintaining these conditions is crucial for preserving the complex tertiary structure of enzyme molecules, which, in turn, is essential to prevent active site alterations that could result in diminished catalytic competence [10]. Such alterations might be manifested in the low performance of key economic indicators [11]. Furthermore, given the relatively high costs associated with enzymes, the development of strategies for recovery and reuse after biotransformations have become the focus of numerous recent research studies [9].

Enzyme immobilization is a route to address this challenge, with the primary objectives of enhancing enzyme stability and facilitating separation from the products and/or substrates present in the reaction mixture [12]. Over the past 50 years, researchers have developed various enzyme immobilization methods, with covalent binding, non-covalent binding, and encapsulation being the most popular [12]. Each method presents its own advantages and disadvantages, primarily in terms of immobilization and activity yield, mass transfer, and operational stability. Covalent enzyme immobilization typically involves the formation of stable covalent bonds between enzyme molecules and solid supports [9,13]. The resulting complexes can be recovered through centrifugation or filtration. Recently, recovery efficiency has been enhanced by employing stimuli-responsive supports that react to applied stimuli, such as magnetic or electric fields or changes in pH or temperature [14–18]. Although micron-sized porous and non-porous materials are common supports, nanostructured materials have emerged as attractive alternatives. These materials exploit high surface-to-volume ratios to accommodate large numbers of immobilized enzyme molecules in smaller volumes, leading to the miniaturization and optimization of bioreactors.

The common nanostructured materials used in enzyme immobilization include silica, zirconia, gold, and iron oxide nanoparticles. Recently, polymeric (e.g., chitosan and gelatin) and carbon-based (e.g., graphene oxide and carbon quantum dots) nanomaterials have gained significant attention [19–21]. Among iron oxide nanoparticles, magnetite stands out due to its strong responsiveness to magnetic fields, ease of synthesis and functionalization, and low toxicity [18,21]. Magnetite nanoparticles (MNPs) can be separated from complex mixtures using magnetic fields but are susceptible to air oxidation and aggregation in aqueous media [15]. This has been addressed by functionalizing the surface

with organosilane molecules (e.g., 3-aminopropyl triethoxysilane (APTES)) and polymeric spacers (e.g., polyethylene glycol (PEG) and polyether amines (PEA)) [15,22,23].

Following functionalization, the introduced functional groups can be used to conjugate enzyme molecules through cross-linking agents, such as glutaraldehyde or carbodiimides [24]. Glutaraldehyde has two reactive aldehyde groups that readily react with amine groups to form imine bonds, while carbodiimides form amide bonds between terminal carboxyl (-COOH) and amine groups (-NH_2) [24]. Invertase immobilization has been reported using conducting polymers with an N-pyrrolyl matrix through electrochemical polymerization, achieving an operational stability of 30 batch cycles [25]. Conducting copolymer matrices of 3-methyl-thienyl methacrylate have been used via potential electrolysis, achieving 20 batch reuses with minimal activity loss [26].

Invertase immobilization on chitosan-coated sol–gel-derived $\gamma - Fe_2O_3$ magnetic nanoparticles has shown superior catalytic performance and enhanced enzyme stability in response to pH and temperature fluctuations. The immobilized enzyme reached 20 batch reuses without significant activity loss [27]. Romero-Vargas and Reyes-Cuellar reportedly conducted the immobilization of invertase on cobalt ferrite magnetic nanoparticles functionalized with chitosan and activated with glutaraldehyde. Cobalt ferrite magnetic nanoparticles functionalized with chitosan and activated with glutaraldehyde have been used to immobilize invertase, presenting a slight reduction in the maximum reaction rate and an increase in the affinity constant (K_M) while maintaining over 91.79% of their original activity after three reuses [28]. Magnetic diatomaceous earth nanoparticles were also used for invertase immobilization, retaining 83% activity after 120 days of storage and increasing their thermal stability by 14% relative to that of the free enzyme, with 60% residual activity after 10 reuse cycles [14].

Although immobilized invertase on MNP has promising attributes, such as an enhanced stability and potential recovery via magnetic-field-induced precipitation, studies focusing on optimal performance in complex mixtures for the hydrolysis and transfructosylation of FOS remain scarce. Numerous modeling studies have examined the kinetics of free and immobilized enzymes catalyzing sucrose hydrolysis [29–32], but few have reported and modeled the hydrolysis and transfructosylation kinetics of the enzymes involved in FOS production [1,6,33]. Other reports contain empirical methods modified to trace the FOS production response [34,35]. Even fewer studies have adjusted FOS production models specifically for immobilized enzymes [36].

This work aims to model the effects of immobilization on enzyme performance in FOS synthesis and the addition of free glucose oxidase to mitigate glucose inhibition. The approximation of the immobilized model is based on minimizing the square residuals of the concentration profiles in a pre-existing kinetic model and the proposed immobilized model in a batch reactor. The obtained model is then applied to continuous reactor modeling (CSTR) and coupled with a model describing the kinetics of free glucose oxidase to examine glucose inhibition mitigation in FOS synthesis using immobilized invertase.

The limitations of this model include its development based solely on literature reports, requiring eventual corroboration with experimental results. This simplified model assumes that all reactions follow the elemental reaction law and that the enzyme's performance on hydrolysis after immobilization is similar to its performance during transfructosylation. Furthermore, this model is a numerical approximation of a kinetic model, and the proximity of the obtained answer to the absolute minimum of the function depends on the robustness and accuracy of the employed numerical method. Despite these considerations, the obtained kinetic model generates sugar concentration profiles similar to those observed in other literature reports, exhibiting the typical progression of the studied enzymatic reaction.

Despite the promising attributes of immobilizing invertase on magnetite nanoparticles, studies focusing on optimal performance in complex mixtures for the hydrolysis and transfructosylation of FOS remain scarce. This work aims to address this gap by modeling the effects of immobilization on enzyme performance in FOS synthesis and the addition of free glucose oxidase to mitigate glucose inhibition.

Section 2 presents the modeling approach used in this study, including hydrolysis and transfructosylation reaction modeling, kinetic parameters sensitivity analysis, immobilized kinetic parameter estimation, CSTR modeling, and glucose inhibition modeling. Section 3 presents the results and discussion of our study, including the hydrolysis and transfructosylation reactions, kinetic parameters sensitivity analysis, immobilized kinetic parameter estimation, CSTR modeling, and glucose inhibition modeling. Finally, Section 4 concludes the paper and provides suggestions for future research.

2. Modeling Approach

2.1. Hydrolysis and Transfructosylation Reaction Modeling

Figure 1 shows the overall synthesis scheme for FOSs, as reported by Vega et al. [6]. This scheme focuses on FOS production using Rohapect CM (AB Enzymes GmbH), a commercially available cellulolytic enzyme preparation. Although this model was not designed for FOS synthesis by invertase (SInv), it demonstrates the complexity of FOS production and offers insights into the mechanisms underlying the generation of the three primary FOSs in such enzyme-mediated processes. In the case of Rohapect CM, sucrose hydrolysis is minimal, as the enzyme–fructose (E·F) complex readily forms either the enzyme–fructose–sucrose (E·FS) complex or the enzyme–fructofuranosylnystose (E·FN) complex, preventing the release of a fructose unit. Furthermore, this enzyme cocktail tends to reform the glycosidic bond, converting glucose and fructose back into sucrose, making this reaction reversible. These factors are not negligible in FOS production with SInv. When employing this enzyme for FOS synthesis, the release of fructose due to hydrolysis and the regeneration of the glycosidic bond are significant.

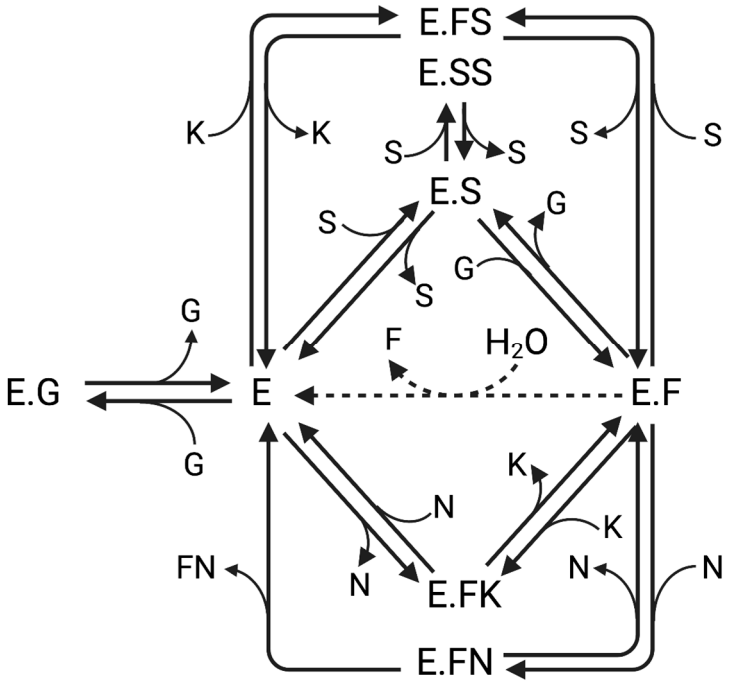

Figure 1. Reaction mechanism for the synthesis of FOSs from sucrose using Rohapec CM. S denotes sucrose, G denotes glucose, F denotes fructose, K denotes 1-kestose, N denotes nystose, FN denotes fructofuranosylnystose, and E denotes unbounded enzyme (adapted from Vega et al. [6]).

A simplified model of this type of process is essential for a comprehensive understanding of the reaction progression, particularly for characterizing the dynamics of this nanobiocatalyst to industrialize this complex reaction. Khandekar et al. proposed a streamlined reaction

system to model the production of FOSs using SInv, aiming to elucidate the behavior of this enzymatic system under various conditions [1] (Equation (1) to Equation (5)).

$$E + Suc \underset{k_{-1}}{\overset{k_1}{\rightleftharpoons}} ESuc \quad (1)$$

$$ESuc \underset{k_{-2}}{\overset{k_2}{\rightleftharpoons}} EFru + Glu \quad (2)$$

$$EFru \underset{k_{-3}}{\overset{k_3}{\rightleftharpoons}} E + Fru \quad (3)$$

$$EFru + Suc \underset{k_{-4}}{\overset{k_4}{\rightleftharpoons}} E + FOS \quad (4)$$

$$E + Glu \underset{k_{-5}}{\overset{k_5}{\rightleftharpoons}} EGlu \quad (5)$$

The proposed model considerably streamlines the depiction of the reaction mechanism layout illustrated in Figure 1. As observed in Equation (4), it consolidates the production of all FOSs into a single reaction. This simplification substantially reduces the number of constants needed to describe the model without making severe assumptions or excluding any significant reactions occurring during FOS synthesis. Importantly, as reported by several studies, this model incorporates a reaction that accounts for glucose inhibition, a significant obstacle to FOS production. Furthermore, it assumes that all reactions follow a first-order mechanism. This system of reactions is subsequently translated into differential equations that model the concentration change of all products and intermediate associations within a batch reactor as a function of time (Equation (6) to Equation (13)) [1].

$$\frac{d[E]}{dt} = -k_1[E][Suc] + k_{-1}[ESuc] + k_3[EFru] - k_{-3}[E][Fru] + k_4[EFru][Suc] - k_{-4}[E][FOS] - k_5[E][Glu] + k_{-5}[EGlu] \quad (6)$$

$$\frac{d[ESuc]}{dt} = k_1[E][Suc] - k_{-1}[ESuc] - k_2[ESuc] + k_{-2}[EFru][Glu] \quad (7)$$

$$\frac{d[EFru]}{dt} = k_2[ESuc] - k_{-2}[EFru][Glu] - k_3[EFru] + k_{-3}[E][Fru] - k_4[EFru][Suc] + k_{-4}[E][FOS] \quad (8)$$

$$\frac{d[EGlu]}{dt} = k_5[E][Glu] - k_{-5}[EGlu] \quad (9)$$

$$\frac{d[Suc]}{dt} = -k_1[E][Suc] + k_{-1}[ESuc] - k_4[EFru][Suc] + k_{-4}[E][FOS] \quad (10)$$

$$\frac{d[Glu]}{dt} = k_2[ESuc] - k_{-2}[EFru][Glu] - k_5[E][Glu] + k_{-5}[EGlu] \quad (11)$$

$$\frac{d[Fru]}{dt} = k_3[EFru] - k_{-3}[E][Fru] \quad (12)$$

$$\frac{d[FOS]}{dt} = k_4[EFru][Suc] - k_{-4}[E][FOS] \quad (13)$$

The model effectively represents the observed behavior of free invertase during FOS production [1]. More intricate models involving substrate specificity constants [6], or diffusion and effectiveness factors, particularly valuable in immobilized enzyme reactions [37], necessitate additional information obtainable or estimable from experimental data.

Nonetheless, to the best of our knowledge, these parameters have not been thoroughly investigated for invertase kinetics, limiting further modeling, particularly for immobilized

systems. Consequently, Michaelis–Menten parameters ($V = V_{max} \times [S]/([S] + K_M)$) were integrated into the simplified kinetic model proposed by Khandekar et al., originally developed to examine free SInv reactions in FOS formation [1]. To adapt this model for both free and immobilized invertase, it required modification with new Michaelis–Menten constants and optimization techniques. Rigorous studies on the kinetics of invertase (or immobilized enzymes) in FOS synthesis remain scarce. As this reaction has been extensively investigated for both free and immobilized invertase, unlike transfructosylation, the model modification relied on literature reports referring to sucrose hydrolysis performed by immobilized and free invertase. This indicates that the modified model presumes that the kinetic changes due to invertase immobilization in the hydrolysis reaction have similar effects on enzyme kinetics during transfructosylation.

To accurately model the change in the kinetics of a system caused by enzyme immobilization, information on the enzyme's performance before and after immobilization was required. Khandekar et al.'s model does not assess immobilization, so Michaelis–Menten constant pairs describing the enzyme's performance on sucrose hydrolysis under both free and immobilized conditions had to be obtained from published studies and incorporated into the model [1]. Valerio et al. reported these constant pairs for free and immobilized SInv: K_M = 0.0657 M and Vmax = 0.0278 M·s^{-1}, and K_M = 0.2057 M and Vmax = 0.0305 M·s^{-1}, respectively [13]. SInv was immobilized on chitosan nanoparticles prepared using the ionotropic method and activated with glutaraldehyde [13]. These constants were chosen for two primary reasons: first, their magnitudes are consistent with those reported in other enzyme immobilization studies [31,32]; second, the covalent binding of enzymes on a glutaraldehyde-activated chitosan nanoparticle surface is significantly similar to the proposed method of coating magnetic nanoparticles in the current investigation.

Initially, the model was modified to represent the reaction kinetics for the free enzyme. Since the chosen Michaelis–Menten constants only represent the hydrolysis reaction, only the reactions associated with sucrose hydrolysis were modified (Equations (1) and (2)). As previously mentioned, the Michaelis–Menten model's elemental definitions were used to modify the model. This assumption implies that the concentration of the enzyme–substrate complex (ES, shown in Equation (14) for the general model, or ESuc, shown in Equation (15) for the invertase-specific model) remains relatively constant and does not vary as a function of time.

$$E + S \underset{k_r}{\overset{k_f}{\rightleftharpoons}} ES \overset{k_{Cat}}{\rightarrow} E + P \tag{14}$$

$$E + Suc \underset{k_{-1}}{\overset{k_1}{\rightleftharpoons}} ESuc \underset{k_{-2}}{\overset{k_2}{\rightleftharpoons}} EFru + Glu \tag{15}$$

The quasi-steady state requires an analytical expression to calculate K_M, as demonstrated in Equation (16). Furthermore, as previously mentioned, transfructosylation occurs when high concentrations of sucrose are present in the medium. In a Michaelis–Menten system operating at elevated substrate concentrations, the relationship [S]/([S] + KM) becomes independent of the substrate, making this assumption valid for the proposed system. Consequently, these types of systems tend to approach their maximum rate, as defined by Equation (17), where $[E_0]$ represents the initial enzyme concentration in the reaction vessel.

$$K_M = \frac{k_r + k_{Cat}}{k_f} \tag{16}$$

$$V_{max} = \frac{k_{Cat}}{[E_0]} \tag{17}$$

$$E + Suc \underset{k_{-1}}{\overset{k_1}{\rightleftharpoons}} ESuc \overset{k_2}{\rightarrow} EFru + Glu \tag{18}$$

The Michaelis–Menten model assumes the reaction producing both the product and the enzyme to be irreversible. Technically, this assumption is not accurate; however,

when the substrate concentration is significantly greater than the product concentration (i.e., [S] >> [P]), this assumption is suitable and allows for the generation of analytical expressions to calculate the concentration of all species involved in the reaction. To determine the kinetic constants k_1 and k_2 of the free enzyme, Equation (15) was assumed to proceed as shown in Equation (18). Given the system's Michaelis constant (K_M), maximum reaction rate (V_{max}), and initial enzyme concentration [E_0] and the reverse kinetic coefficient of the first reaction (k_r), Equations (16) and (17) can be used to solve k_f and k_{Cat} (i.e., k_1 and k_2, or k_{-1}). In this case, the Michaelis–Menten constants were known, the initial enzyme concentration was assumed to be 2.78×10^{-4} M, and k_{-1} was assumed to correspond to the value reported by Khandekar et al. (0.040 s^{-1}) [1]. The remaining model constants (k_{-2}, k_3, k_{-3}, k_4, k_{-4}, k_5, and k_{-5}) were assumed to be equivalent to those previously reported. Table 1 shows the results of the constants derived from this approximation. In our CSTR modeling, we maintained this assumption by controlling the feed rate of the substrate and the dilution rate of the reactor. However, it is important to note that this assumption may not always be valid for all conditions and should be carefully evaluated when modeling a CSTR.

Table 1. Kinetic constants for the free and immobilized models.

Parameters	Free	Immobilized
$k_1\left[(Ms)^{-1}\right]$	1525.72	1485.41
$k_{-1}\left[s^{-1}\right]$	0.04	195.75
$k_2\left[s^{-1}\right]$	100.20	109.80
$k_{-2}\left[(Ms)^{-1}\right]$	26.02	4.46
$k_3\left[s^{-1}\right]$	13.57	11.26
$k_{-3}\left[(Ms)^{-1}\right]$	43.20	35.16
$k_4\left[(Ms)^{-1}\right]$	1.96	1.91
$k_{-4}\left[(Ms)^{-1}\right]$	80.10	81.41
$k_5\left[(Ms)^{-1}\right]$	1.15×10^{-5}	0.00
$k_{-5}\left[s^{-1}\right]$	7.79	7.80

After adjusting the hydrolysis-associated kinetic constants to the new Michaelis–Menten system, the differential equation system described by Equation (6) to Equation (13) is fully defined, representing the concentration change of all species over time in a batch reactor. Note that the formulation of all rates was based on the assumption that all reactions follow the elementary reaction rate law. This system of simultaneous differential equations was solved using the ODE15s solver in MATLAB®®. This ordinary differential equation solver was chosen due to the described system of equations being particularly stiff, i.e., numerically unstable, unless an extremely small step size is employed to solve the system. A stiff differential equation is one where the desired solution changes slowly, while other nearby solutions change rapidly, necessitating a very small step size to converge to the correct solution [38].

2.2. Kinetic Parameters Sensitivity Analysis

To gain a better understanding of the model's behavior, we conducted a sensitivity analysis to investigate the influence of each kinetic constant on the final concentration of FOS (FOS_{end}) after 1600 s, the maximum concentration of FOS (FOS_{max}), and the time at which the maximum concentration of FOS occurs (t_{FOSmax}).

2.3. Immobilized Kinetic Parameter Estimation

The immobilized kinetic parameters were estimated by minimizing the sum of the squared residuals of the FOS concentration profile obtained from the immobilized enzymatic system and the kinetic constants relative to the free enzyme concentration profile and modeling parameters, respectively. Following Valerio et al.'s study, the immobilized kinetic parameters were calculated to match the behavior of the free enzyme, assuming that this behavior remains consistent during immobilization [13]. Our findings suggest that immobilization does not affect the optimal conditions, yields, or enzymatic activities and that the one-point immobilized enzymatic system displays profiles similar to those of free biocatalysts [13]. This is consistent with the findings reported by Garcia-Galan et al. [39]. This estimation was carried out using the MATLAB®® function *fmincon*. To prioritize the similarity between the free and immobilized FOS profiles in the objective function of minimization, we reduced the weight of the sum of the squared residual term associated with the kinetic parameters by multiplying it by a controlling scalar.

Furthermore, we constrained the estimation to adhere to the known immobilized invertase kinetics by limiting the resulting constants to follow Equations (16) and (17) for the previously stated immobilized Michaelis–Menten parameters, consistent with the K_M and V_{max} values reported by Valerio et al. [13]. The immobilized kinetic parameters obtained from this estimation are listed in the second column of Table 1, arranged according to the set of reactions defined by Equations (1) to (5). Notably, the kinetic parameters that exhibit negligible effects on FOS concentration profile properties (particularly the maximum FOS concentration and the time at which it occurs), according to the sensitivity analysis, show the most significant variation in terms of free enzyme kinetics.

2.4. CSTR Modeling

We characterized the continuous reaction by simulating an ideal CSTR reactor operating at 55°C, which is the optimal condition for the given kinetic parameters, as reported by Khandekar et al. and Valerio et al. [13]. The continuous operation was modeled for dilution rate (D) values ranging from 0 to 50 h^{-1} (0.02 to ∞ h in residence time (τ) equivalency). We solved a set of design balances defined by Equation (19) for each dilution rate value, repeatedly for each of the reactants and products considered in batch modeling. The resulting system of algebraic equations was solved using MATLAB's fsolve function.

$$C_i = C_{0,i} + \frac{r_i}{D} \rightarrow C_i = C_{0,i} + \tau * r_i \quad (19)$$

In Equation (19), C_i and $C_{0,i}$ represent the final and inlet concentrations of species *i*, respectively. For each species *i*, the reaction rate r_i is described by the right-hand side expression of the corresponding batch modeling differential equation (Equation (6) to Equation (13)). The resulting exiting concentrations yielded a profile for each of the sugars involved in the reactive system as a function of the dilution rate, enabling us to determine the optimal dilution rate for CSTR operation and the corresponding maximum exiting FOS concentration. We specified the initial concentrations of sucrose and invertase as 1.53 M (525 g/L is the optimal value reported by Khandekar et al. [1]) and 2.78×10^{-4} M, respectively. We assumed the absence of all other species in the reactor's feed stream.

2.5. Glucose Inhibition Modeling

Glucose inhibition is a major obstacle to achieving high FOS production rates using SInv. One possible solution to this challenge is to remove glucose from the reaction medium, which would enhance the accessibility of the enzyme to hydrolysis and transfructosylation. Glucose oxidase (GOx), a commonly used enzyme in patient blood assays to detect glucose levels, has well-established reaction kinetics that can be leveraged for this purpose. By oxidizing glucose, GOx produces hydrogen peroxide (H_2O_2), which leads to a slight decrease in pH (around 5 at a 10% concentration), which is the optimal pH for SInv activity. It is important to note that, while the production of hydrogen peroxide (H_2O_2) during

glucose oxidation may only slightly decrease the pH, the formation of glucono-d-lactone (d-lac) can have a stronger impact on the pH. This is because d-lac is partially hydrolyzed in water to form gluconic acid, which can significantly affect the pH, especially at high substrate concentrations (e.g., 1.5 M). This needs to be considered when modeling the glucose inhibition process. Immobilizing GOx on magnetic nanoparticles could further enhance its potential for use in the FOS production process by improving its recovery after reaction cycles, thus reducing costs and increasing biocatalyst productivity. During glucose oxidation in the presence of dissolved oxygen, GOx undergoes a series of redox reactions. First, oxidized GO_x (E_{OX}) oxidizes glucose, forming a reduced enzyme (E_{red}) and glucono-δ-lactone (δ-lac)) complex (Equation (20)). The dissociation of this complex is shown in Equation (21). Then, dissolved oxygen re-oxidizes E_{red} to produce the $E_{ox}(H_2O_2)$ complex (Equation (22)). Lastly, this complex dissociates, as illustrated by Equation (23) [40].

$$E_{ox} + Glu \xrightarrow{k_1^g} E_{red}(\delta - lac) \quad (20)$$

$$E_{red}(\delta - lac) \xrightarrow{k_2^g} E_{red} + \delta - lac \quad (21)$$

$$E_{red} + O_2 \xrightarrow{k_3^g} E_{ox}(H_2O_2) \quad (22)$$

$$E_{ox}(H_2O_2) \xrightarrow{k_4^g} E_{ox} + H_2O_2 \quad (23)$$

The superscript g denotes the kinetic constants for glucose oxidation. According to Tao et al. [40] and Gibson et al. [41], the concentrations of E_{red}(δ-lac) and $E_{OX}(H_2O_2)$ are small enough, and k_2^g and k_4^g are more significant than the hypothetical reverse reaction rates k_{-1}^g and k_{-3}^g, making the reactions irreversible.

The rate constants for glucose oxidation with GO_x at 38 °C were obtained from Gibson et al. [41] and are shown in Table 2. Since k_2^g was not reported at the selected temperature, it was extrapolated using the interp1 function of MATLAB®® based on values at lower temperatures. It is important to note that these kinetic constants refer to free (not immobilized) GOx, and the models below assume systems with immobilized invertase and free GOx.

Table 2. Kinetic constants for the reaction glucose oxidase.

Parameters	Value [41]
$k_1^g\left[(Ms)^{-1}\right]$	1.6×10^4
$k_2^g\left[(s)^{-1}\right]$	8.4×10^3
$k_3^g\left[(Ms)^{-1}\right]$	2.4×10^6
$k_4^g[s^{-1}]$	2000

2.6. Glucose Inhibition: Batch Model

The net reaction rates were defined using Equations (20)–(23), assuming that all reactions follow the elemental rate law. To relax the numerical problem, the dissolved oxygen concentration was assumed to be constant (zero) in a differential representation. To account for glucose inhibition mitigation, the previously defined immobilized invertase system (Equations (6)–(13)) was coupled with Equations (24)–(31) to create a new batch model. The resulting system of differential equations, with a dimension of 15 × 15, was solved using MATLAB®®'s ODE solver.

$$\frac{d[E_{ox}]}{dt} = k_4^g[E_{ox}(H_2O_2)] - k_1^g[E_{ox}][Glu] \quad (24)$$

$$\frac{d[E_{red}]}{dt} = k_2^g[E_{red}(\delta - lac)] - k_3^g[E_{red}][O_2] \quad (25)$$

$$\frac{d[E_{red}(\delta - lac)]}{dt} = k_1^g[E_{ox}][Glu] - k_2^g[E_{red}(\delta - lac)] \quad (26)$$

$$\frac{d[E_{ox}(H_2O_2)]}{dt} = k_3^g[E_{red}][O_2] - k_4^g[E_{ox}(H_2O_2)] \quad (27)$$

$$\frac{d[\delta - lac]}{dt} = k_2^g[E_{red}(\delta - lac)] \quad (28)$$

$$\frac{d[O_2]}{dt} = 0 \quad (29)$$

$$\frac{d[H_2O_2]}{dt} = k_4^g[E_{ox}(H_2O_2)] \quad (30)$$

Equation (11), which represents the differential equation for glucose, was modified by adding a term to account for its consumption in the new reaction represented by Equation (20). The resulting equation, Equation (31), represents the differential equation for glucose in the batch model.

$$\frac{d[Glu]}{dt} = \ldots - k_1^g[E_{ox}][Glu] \quad (31)$$

2.7. Glucose Inhibition: CSTR Model

In the CSTR model, based on the immobilized invertase model, seven additional equations were included relating to the new species involved in glucose oxidation. These equations were defined by Equation (19), with the reaction rate defined as the RHS expression in the corresponding differential equations for the new species represented in Equations (24)–(30). The glucose reaction rate was modified by inserting a new term addressing the new glucose-containing reaction. The same iterative procedure and initial concentrations were used for the CSTR modeling.

3. Results and discussion

3.1. Hydrolysis and Transfructosylation Reaction

Figure 2 illustrates the obtained profiles that align with the simulation results reported by Khandekar et al., whose original model was adapted to include the calculated Michaelis–Menten kinetic parameters for the sucrose hydrolysis reaction [1]. Khandekar et al.'s research demonstrates an excellent correlation between the experimental and simulated results (obtained by COPASI simulation) [1]. Consequently, the latter's resemblance to the profiles shown in Figure 2 suggests that the modified kinetic model proposed in this study maintains an excellent fit for the experimental behavior. A similar trend has been observed in other modeling works on the production of resveratrol, cephalosporin C, and inulinase [42–44]. As anticipated, almost all sucrose is consumed because it is either hydrolyzed, yielding fructose and glucose, or consumed in the transfructosylation reaction. Since fructose is also consumed in the transfructosylation reaction, its production rate is typically lower than that of glucose. In addition, the production of FOS follows a convex curve over time. The latter indicates that the maximum production of FOS occurs after approximately 6.6 min of a continuous reaction. However, FOSs are later consumed to produce fructose and sucrose, which are eventually hydrolyzed. After both reactions have consumed sufficient sucrose, the system tends to favor hydrolysis over transfructosylation and even consumes FOS to regenerate sucrose and continue its hydrolysis. This behavior is well documented [45].

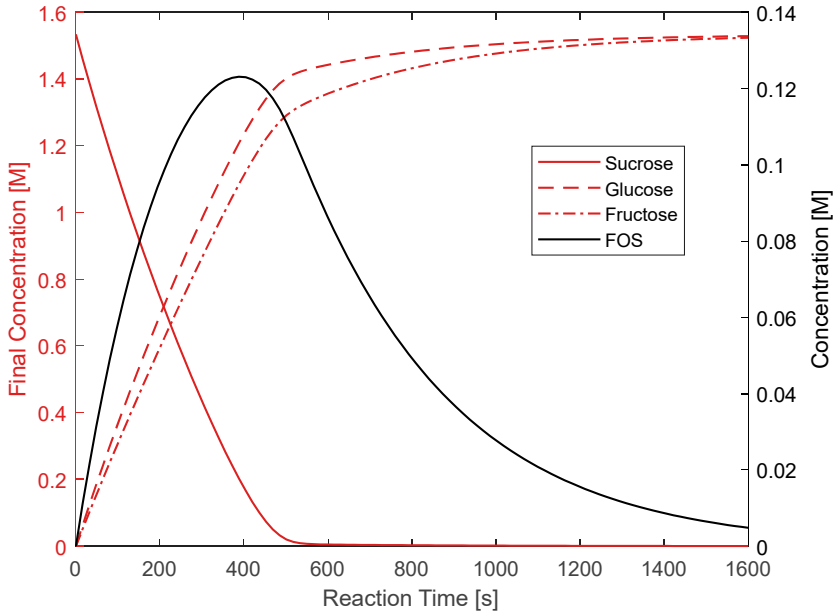

Figure 2. Sugar concentration profiles as a function of batch reactor time for the free enzyme.

3.2. Kinetic Parameters Sensitivity Analysis

To gain a deeper understanding of the model's behavior, a sensitivity analysis was conducted to determine the impact of each kinetic constant on the final concentration of FOS (FOS_{end} after 1600 s), the maximum concentration of FOS (FOS_{max}), and the time at which the maximum concentration of FOS occurs (t_{FOSmax}). The equations were individually solved after increasing each constant by one order of magnitude. Figure 3 shows the results for all three variables when modifying each constant. Sensitivity analyses have been employed in other works to understand the impact of kinetic constants [46,47].

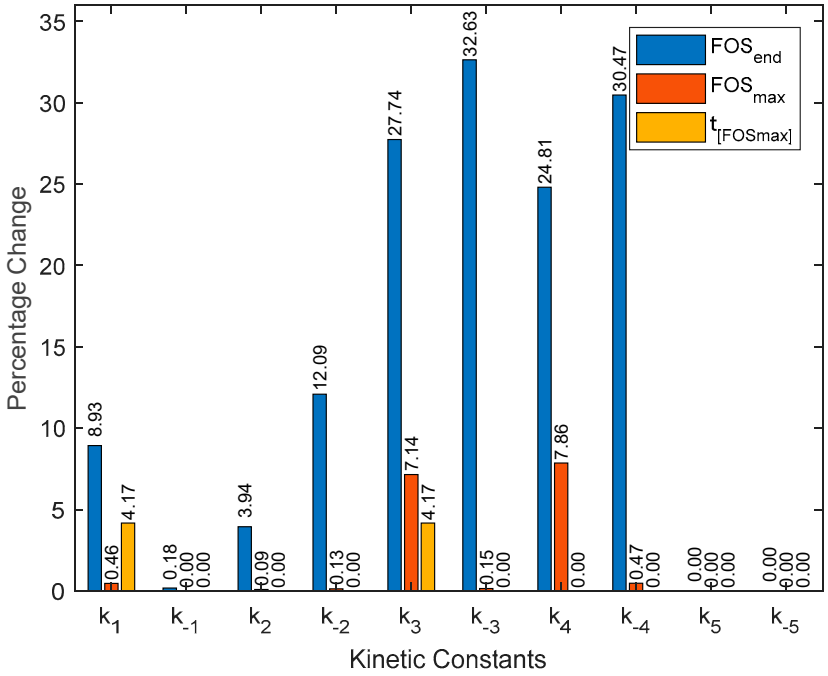

Figure 3. Kinetic constants sensitivity analysis results.

This analysis suggests that FOSend is the variable most affected by fluctuations in the kinetic parameters. This value is influenced primarily by k_1, k_{-2}, k_3, k_{-3}, k_4, and

k_{-4}. However, this result could be disregarded because FOSend is a variable that can be easily manipulated by stopping the reaction at tFOSmax. Moreover, FOSmax is primarily influenced by k_3 and k_4 to a comparable extent. Furthermore, k_1, k_{-3}, and k_{-4} have a negligible (or even nonexistent) impact on FOSmax. tFOSmax is the variable least affected by fluctuations in the kinetic constants, with k_1 and k_3 being insensitive to this value. In conclusion, the constants that affect FOSmax and tFOSmax the most are primarily those associated with the forward reaction of fructose detachment from the enzyme (shown in Equation (3)) and the forward reaction of FOS production (Equation (4)). These results indicate that FOS production (using the proposed model) heavily relies on the stability of the enzymatic complex EFru in the reactive media and its coupling with a sucrose acceptor.

3.3. Immobilized Kinetic Parameter Estimation

The kinetic constant with the greatest variation (k_{-1}) counteracted the change in the hydrolysis-related Michaelis–Menten parameters between the free and immobilized enzymes, satisfying the known kinetic restriction specified alongside the estimation method. In addition, the glucose inhibition reaction (Equation (5)), whose parameters are associated with the minimum impact on FOS profile properties, became irrelevant as its associated forward kinetic parameter became null. Figure 4 depicts the profiles of both the free and immobilized FOS concentrations, demonstrating that the estimated immobilized kinetic parameters in the batch reaction model provide a satisfactory fit. The estimation of immobilized kinetic parameters has been reported to be crucial in other studies involving immobilized enzymes, such as urease, β-galactosidase, and glucose oxidase [25,48,49].

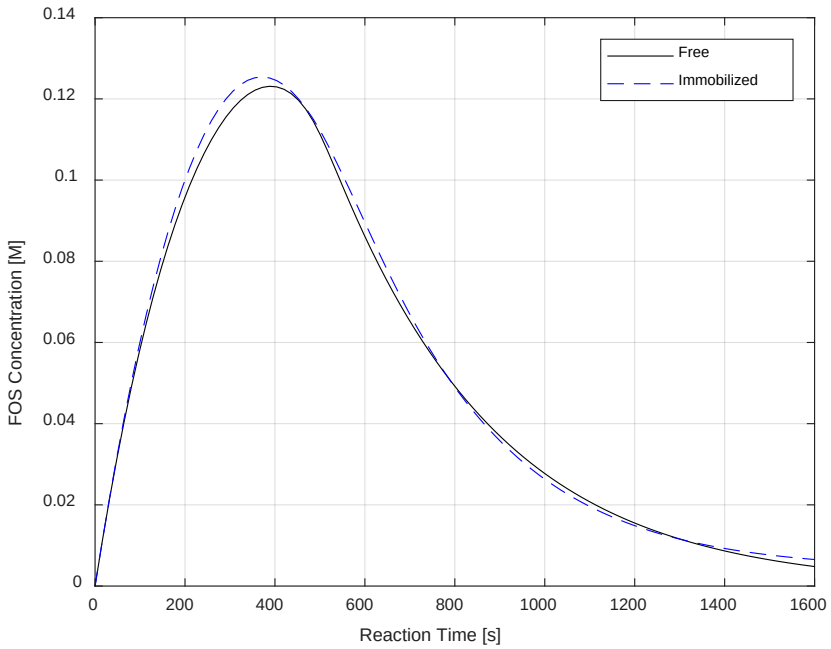

Figure 4. FOS concentration profile as a function of batch reaction time for free and immobilized enzyme systems.

3.4. CSTR Modeling

The sucrose, fructose, glucose, and FOS exiting concentrations as a function of the dilution rate are shown in Figure 5, with the optimal dilution rate at 14.2 h^{-1} (τ = 4.22 min) and the maximum FOS concentration corresponding to 0.074 M. Other modeling works on gluconic acid and chitooligosaccharide production, and pectate digestion using immobilized enzymes in CSTR systems have reported similar concentration profiles [50–52].

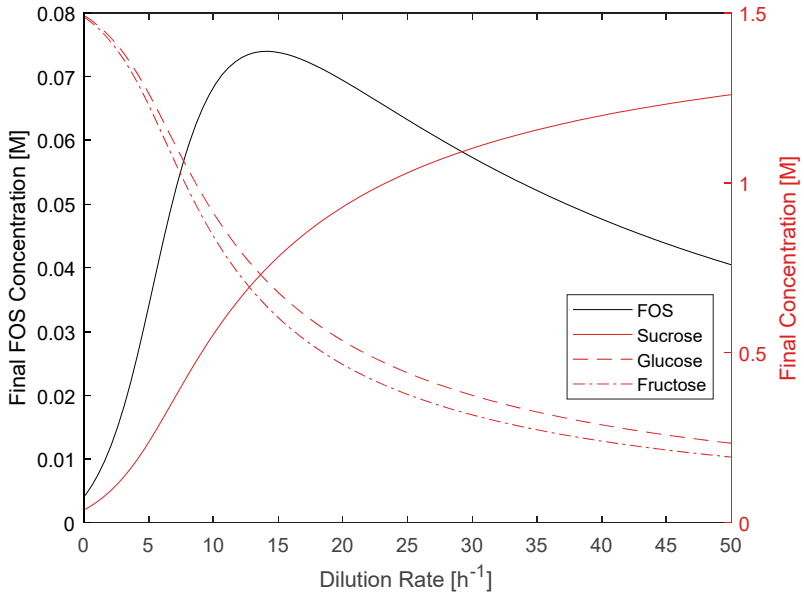

Figure 5. Final sugar concentrations in a CSTR as a function of dilution rate for immobilized invertase system.

All profiles exhibited the expected behavior in which a high dilution rate (i.e., a short residence time) resulted in a decrease in monosaccharide and FOS output, and a further reaction time beyond the optimal value resulted in an increase in the fructose and glucose production rate via FOS consumption via hydrolysis. The infinite theoretical reaction exhibits a minimum FOS concentration within the evaluation range, where fructose and glucose concentrations are virtually identical, indicating that FOS hydrolysis accelerates fructose production.

3.5. Glucose Inhibition Modeling

3.5.1. Glucose Inhibition: Batch Model

Sucrose, fructose, and FOS profiles similar to those with immobilized invertase are observed in batch models of glucose inhibition with free glucose oxidase insertion (Figure 6A). Due to secondary enzyme oxidation reactions, they also exhibit a predicted constant absence of glucose.

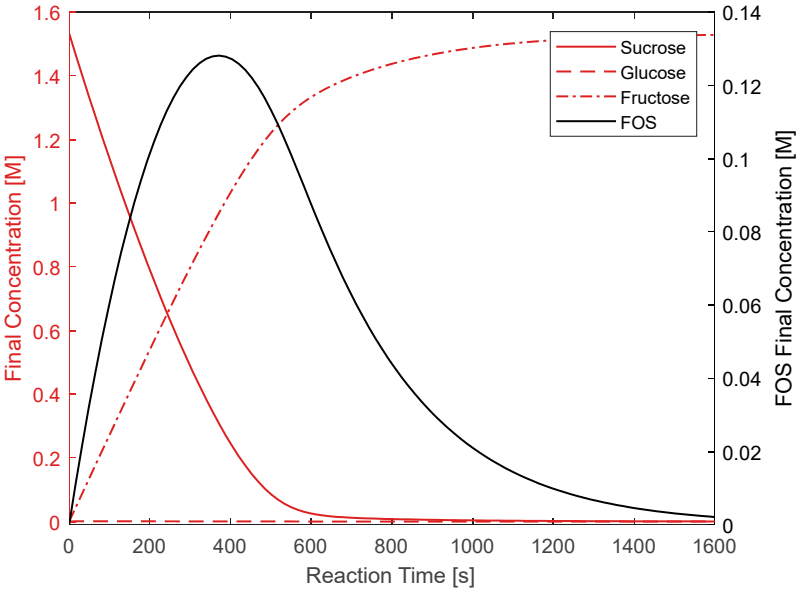

(**A**)

Figure 6. *Cont.*

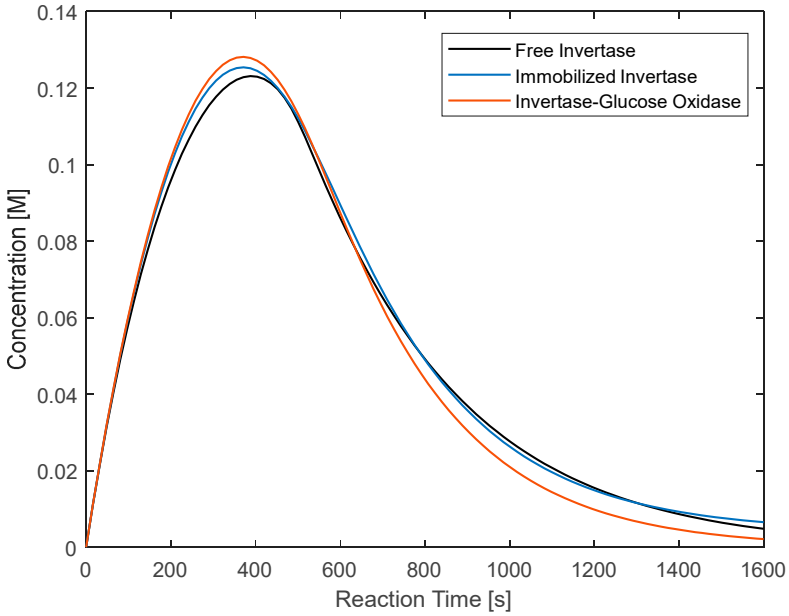

(**B**)

Figure 6. (**A**) Concentration profiles as a function of batch reaction time for immobilized invertase system with glucose oxidase insertion. (**B**) FOS concentration profile as a function of batch reaction time for the free enzyme, immobilized enzyme, and glucose oxidase insertion systems.

The differences and benefits associated with this model are evident in Figure 6B, which demonstrates that the maximum FOS concentration is slightly improved (2.1% increase) due to the improvement of the hydrolysis forward reaction (Equation (2)) as a result of glucose consumption, taking into account chemical equilibrium, which consequently improves enzyme–fructose complex formation, thereby increasing FOS production (Equation (4)). This observation is based on the recognition that the direct effect of the glucose inhibition (Equation (5)) reaction on the system was previously nullified by the kinetic parameter estimation (due to the resulting null value for k_{-5}). Therefore, the maximum FOS concentration increase cannot be attributed to a slower forward kinetic progression of Equation (5) associated with the formation of the glucose–enzyme complex. In addition, glucose oxidase accelerates the FOS hydrolysis that occurs past the optimal operation time due to the accelerated consumption of sucrose.

3.5.2. Glucose Inhibition: CSTR Model

Figure 7 compares the final concentrations of the immobilized invertase reaction (without glucose inhibition control) and immobilized invertase with glucose oxidase insertion as a function of the dilution rate across four different plots. The optimal dilution rate shifted marginally toward a shorter reaction time (relative to the previously determined optimal operation), corresponding to a slight increase in the maximum FOS concentration (1 percent growth regarding previous CSTR modeling). The absence of glucose in the exiting stream results from its constant oxidation. Changes in the sucrose, fructose and FOS profiles nearing an infinite reaction time are attributable to a glucose-deficiency-induced acceleration of sucrose hydrolysis.

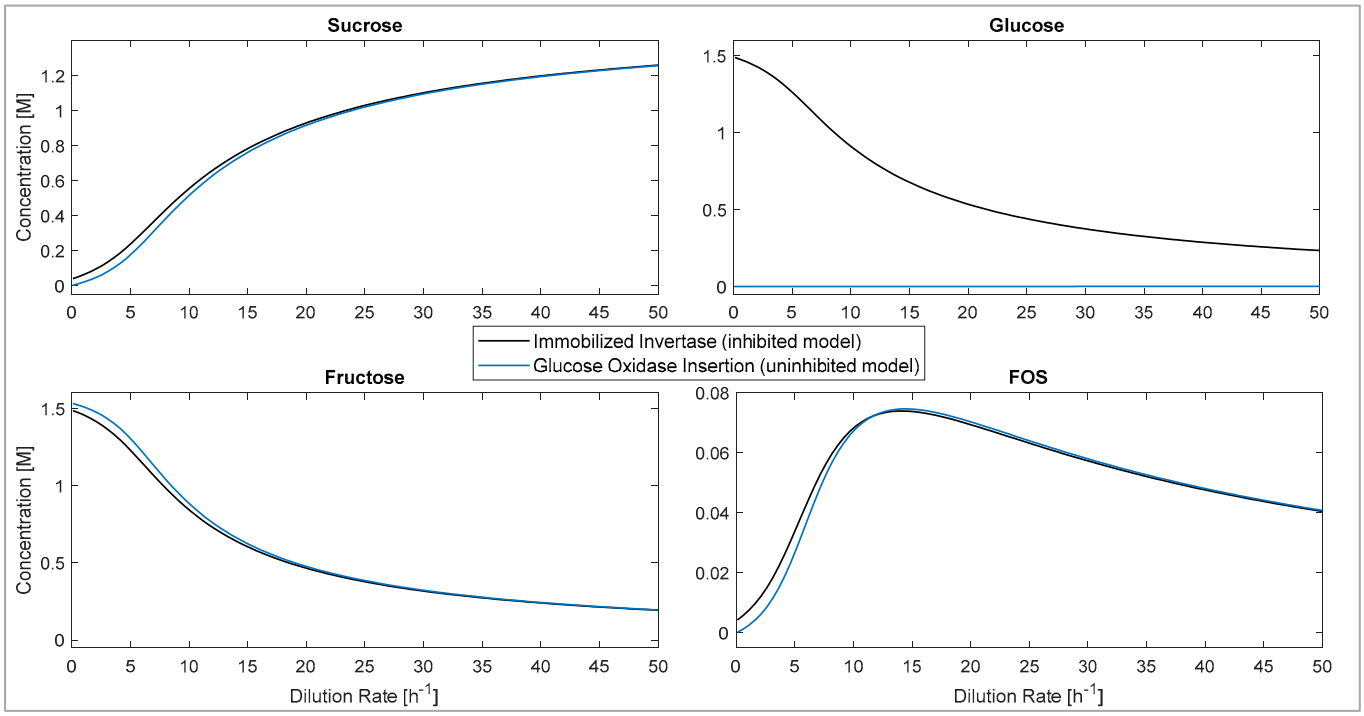

Figure 7. Final concentrations in a CSTR as a function of dilution rate for immobilized invertase and glucose oxidase insertion systems.

4. Conclusions

In this comprehensive theoretical study, we investigated the simulation of optimal fructooligosaccharide (FOS) production with immobilized invertase, focusing on key factors, such as enzyme immobilization, reaction kinetics, and glucose inhibition control. This study employed various modeling techniques, including batch and continuous stirred-tank reactor (CSTR) modeling, to analyze the complex dynamics of FOS production in different configurations. The immobilization of invertase on functionalized magnetite nanoparticles was found to be a promising approach, offering the potential for enhanced reusability and performance. As a result, a theoretical model was developed to estimate immobilized enzyme kinetics using a system of reversible elemental reactions with the intention of guiding future experimental research.

The results of this study suggest that batch reactions are preferred over continuous reactions for optimal FOS production. The batch reaction achieved a maximum FOS concentration of 125.4 mM at an optimal reaction time of 372 s, while the CSTR model reached a maximum FOS concentration of 73.96 mM at a dilution rate of 14.2 h^{-1}. Furthermore, the impact of glucose inhibition on FOS production was explored by incorporating glucose oxidase reactions into the model. The modified batch and continuous reaction models showed a slight increase in the maximum FOS concentration (2.1% and 1%, respectively), indicating that glucose absence in the reaction media had a minimal effect on FOS yield. Nevertheless, further evaluation is required to assess the industrial and economic implications of glucose oxidase inclusion, the constant oxygen feed requirement, and the separation process repercussions due to the synthesis of additional products.

Another important factor to consider when using glucose oxidase (GOx) for glucose conversion is the potential for H_2O_2-dependent enzyme deactivation. The production of hydrogen peroxide (H_2O_2) during glucose oxidation can impact the biotransformation process by deactivating enzymes [53]. This effect may differ in a discontinuous stirred-tank reactor (STR) compared to a CSTR [53]. One potential solution to prevent H_2O_2 accumulation and its negative effects on enzyme activity is the addition of catalase, an enzyme that catalyzes the decomposition of H_2O_2 into water and oxygen [53]. The generation of H_2O_2

with enzymes such as GOx requires co-substrates that are transformed into side products (in the case of GOx, gluconic acid) [54].

In sum, this theoretical study sheds light on the intricate interplay between various factors impacting FOS production with immobilized invertase, highlighting the importance of considering these factors when making decisions about optimizing FOS production. This study also underscores the need for a careful balance between different approaches and the challenges associated with each method. By providing a comprehensive analysis of the key factors, this work contributes to a deeper understanding of the complex process of simulating optimal FOS production with immobilized invertase.

Future work will focus on further optimizing the immobilization process and exploring the use of other types of nanoparticles for enzyme immobilization. Additionally, an experimental validation of the proposed kinetic model and reactor design strategy will be valuable. Finally, investigating the potential for coupling glucose oxidase onto functionalized nanoparticles to minimize glucose inhibition and improve FOS synthesis will also be a fruitful avenue for future research.

Author Contributions: Conceptualization, D.P.M., A.H.B., J.C.C. and L.H.R.; methodology, D.P.M., A.H.B., J.C.C. and L.H.R.; software, D.P.M. and A.H.B.; validation, J.C.C. and L.H.R.; formal analysis, D.P.M., A.H.B., J.C.C. and L.H.R.; investigation, D.P.M. and A.H.B.; resources, J.C.C. and L.H.R.; data curation, D.P.M. and A.H.B. writing—original draft preparation, D.P.M. and A.H.B. writing—review and editing, J.C.C. and L.H.R.; visualization, D.P.M. and A.H.B.; supervision, J.C.C. and L.H.R.; project administration, J.C.C. and L.H.R.; funding acquisition, J.C.C. and L.H.R. All authors have read and agreed to the published version of the manuscript.

Funding: This research received no external funding.

Institutional Review Board Statement: Not applicable.

Informed Consent Statement: Not applicable.

Data Availability Statement: Not applicable.

Conflicts of Interest: The authors declare no conflict of interest.

References

1. Khandekar, D.C.; Palai, T.; Agarwal, A.; Bhattacharya, P.K. Kinetics of sucrose conversion to fructo-oligosaccharides using enzyme (invertase) under free condition. *Bioprocess Biosyst. Eng.* **2014**, *37*, 2529–2537. [CrossRef] [PubMed]
2. Chen, G.; Li, C.; Chen, K. Fructooligosaccharides: A Review on Their Mechanisms of Action and Effects. In *Studies in Natural Products Chemistry*; Elsevier: Amsterdam, The Netherlands, 2016; Volume 48, ISBN 9780444636027.
3. Lafraya, Á.; Sanz-Aparicio, J.; Polaina, J.; Marín-Navarro, J. Fructo-oligosaccharide synthesis by mutant versions of Saccharomyces cerevisiae invertase. *Appl. Environ. Microbiol.* **2011**, *77*, 6148–6157. [CrossRef] [PubMed]
4. Kulshrestha, S.; Tyagi, P.; Sindhi, V.; Yadavilli, K.S. Invertase and its applications—A brief review. *J. Pharm. Res.* **2013**, *7*, 792–797. [CrossRef]
5. Veana, F.; Flores-Gallegos, A.C.; Gonzalez-Montemayor, A.M.; Michel-Michel, M.; Lopez-Lopez, L.; Aguilar-Zarate, P.; Ascacio-Valdés, J.A.; Rodríguez-Herrera, R. Invertase: An enzyme with importance in confectionery food industry. In *Enzymes in Food Technology*; Springer: Singapore, 2018; pp. 187–212. [CrossRef]
6. Vega, R.; Zuniga-Hansen, M.E. A new mechanism and kinetic model for the enzymatic synthesis of short-chain fructooligosaccharides from sucrose. *Biochem. Eng. J.* **2014**, *82*, 158–165. [CrossRef]
7. Avigad, G.; Dey, P.M. *Carbohydrate Metabolism: Storage Carbohydrates*; Academics Press: San Diego, CA, USA, 1997; ISBN 0122146743.
8. Michel, M.R.; Rodríguez-Jasso, R.M.; Aguilar, C.N.; Gonzalez-Herrera, S.M.; Flores-Gallegos, A.C.; Rodríguez-Herrera, R. Fructosyltransferase Sources, Production. In *Probiotics and Prebiotics in Human Nutrition and Health*; InTech: Rijeka, Croatia, 2016. [CrossRef]
9. Gupta, M.N.; Kaloti, M.; Kapoor, M.; Solanki, K. Nanomaterials as matrices for enzyme immobilization. *Artif. Cells Blood Substit. Biotechnol.* **2011**, *39*, 98–109. [CrossRef]
10. Walker, J.M.; Ditor, S.E.E. *Immobilization of Enzymes and Cells*, 2nd ed.; Guisan, J.M., Ed.; Humana Press: Madrid, Spain, 2006; ISBN 1588292908.
11. Robinson, P.K. Enzymes: Principles and biotechnological applications. *Essays Biochem.* **2015**, *59*, 1–41. [CrossRef]
12. Tischer, W.; Kasche, V. Immobilized enzymes: Crystals or carriers? *Trends Biotechnol.* **1999**, *17*, 326–335. [CrossRef]

13. Valerio, S.G.; Alves, J.S.; Klein, M.P.; Rodrigues, R.C.; Hertz, P.F. High operational stability of invertase from Saccharomyces cerevisiae immobilized on chitosan nanoparticles. *Carbohydr. Polym.* **2013**, *92*, 462–468. [CrossRef]
14. Cabrera, M.P.; Assis, C.R.D.; Neri, D.F.M.; Pereira, C.F.; Soria, F.; Carvalho, L.B. High sucrolytic activity by invertase immobilized onto magnetic diatomaceous earth nanoparticles. *Biotechnol. Rep.* **2017**, *14*, 38–46. [CrossRef]
15. Donadelli, J.A.; García Einschlag, F.S.; Laurenti, E.; Magnacca, G.; Carlos, L. Soybean peroxidase immobilized onto silica-coated superparamagnetic iron oxide nanoparticles: Effect of silica layer on the enzymatic activity. *Colloids Surf. B Biointerfaces* **2018**, *161*, 654–661. [CrossRef]
16. Minteer, S.D. Enzyme Stabilization and Immobilization. *Methods Mol. Biol.* **2011**, *679*, 230. [CrossRef]
17. Fortes, C.C.S.; Daniel-da-Silva, A.L.; Xavier, A.M.R.B.; Tavares, A.P.M. Optimization of enzyme immobilization on functionalized magnetic nanoparticles for laccase biocatalytic reactions. *Chem. Eng. Process. Process Intensif.* **2017**, *117*, 1–8. [CrossRef]
18. Ramírez-acosta, C.M.; Cifuentes, J.; Castellanos, M.C.; Moreno, R.J.; Muñoz-camargo, C.; Cruz, J.C.; Reyes, L.H. Ph-responsive, cell-penetrating, core/shell magnetite/silver nanoparticles for the delivery of plasmids: Preparation, characterization, and preliminary in vitro evaluation. *Pharmaceutics* **2020**, *12*, 561. [CrossRef] [PubMed]
19. Torres-Vanegas, J.D.; Cifuentes, J.; Puentes, P.R.; Quezada, V.; Garcia-Brand, A.J.; Cruz, J.C.; Reyes, L.H. Assessing cellular internalization and endosomal escape abilities of novel BUFII-Graphene oxide nanobioconjugates. *Front. Chem.* **2022**, *10*, 974218. [CrossRef]
20. Gonzalez-Melo, C.; Garcia-Brand, A.J.; Quezada, V.; Reyes, L.H.; Muñoz-Camargo, C.; Cruz, J.C. Highly efficient synthesis of type B gelatin and low molecular weight chitosan nanoparticles: Potential applications as bioactive molecule carriers and cell-penetrating agents. *Polymers* **2021**, *13*, 4078. [CrossRef]
21. Ramírez-Acosta, C.M.; Cifuentes, J.; Cruz, J.C.; Reyes, L.H. Patchy Core/Shell, Magnetite/Silver Nanoparticles via Green and Facile Synthesis: Routes to Assure Biocompatibility. *Nanomaterials* **2020**, *10*, 1857. [CrossRef]
22. Popescu, R.C.; Andronescu, E.; Vasile, B.S. Recent advances in magnetite nanoparticle functionalization for nanomedicine. *Nanomaterials* **2019**, *9*, 1791. [CrossRef]
23. Can, K.; Ozmen, M.; Ersoz, M. Immobilization of albumin on aminosilane modified superparamagnetic magnetite nanoparticles and its characterization. *Colloids Surf. B Biointerfaces* **2009**, *71*, 154–159. [CrossRef] [PubMed]
24. Nguyen, H.H.; Kim, M. An Overview of Techniques in Enzyme Immobilization. *Appl. Sci. Converg. Technol.* **2017**, *26*, 157–163. [CrossRef]
25. Gürsel, A.; Alkan, S.; Toppare, L.; Yağci, Y. Immobilization of invertase and glucose oxidase in conducting H-type polysiloxane/polypyrrole block copolymers. *React. Funct. Polym.* **2003**, *57*, 57–65. [CrossRef]
26. Cirpan, A.; Alkan, S.; Toppare, L.; Hepuzer, Y.; Yagci, Y. Immobilization of invertase in conducting copolymers of 3-methylthienyl methacrylate. *Bioelectrochemistry* **2003**, *59*, 29–33. [CrossRef] [PubMed]
27. Waifalkar, P.P.; Parit, S.B.; Chougale, A.D.; Sahoo, S.C.; Patil, P.S.; Patil, P.B. Immobilization of invertase on chitosan coated γ-Fe_2O_3 magnetic nanoparticles to facilitate magnetic separation. *J. Colloid Interface Sci.* **2016**, *482*, 159–164. [CrossRef] [PubMed]
28. Vargas, G.A.R.; Cuellar, J.C.R. Sucrose hydrolysis by invertase of Saccharomyces cerevisiae immobilized on cobalt ferrite magnetic nanoparticles. *Acta Agron.* **2019**, *68*, 115–125. [CrossRef]
29. de Souza Soares, A.; Augusto, P.E.D.; Júnior, B.R.D.C.L.; Nogueira, C.A.; Vieira, É.N.R.; de Barros, F.A.R.; Stringheta, P.C.; Ramos, A.M. Ultrasound assisted enzymatic hydrolysis of sucrose catalyzed by invertase: Investigation on substrate, enzyme and kinetics parameters. *Lwt* **2019**, *107*, 164–170. [CrossRef]
30. Vu, T.K.H.; Le, V.V.M. Biochemical studies on the immobilization of the enzyme invertase (EC.3.2.1.26) in alginate gel and its kinetics. *Int. Food Res. J.* **2008**, *15*, 73–78.
31. Azodi, M.; Falamaki, C.; Mohsenifar, A. Sucrose hydrolysis by invertase immobilized on functionalized porous silicon. *J. Mol. Catal. B Enzym.* **2011**, *69*, 154–160. [CrossRef]
32. Szymańska, K.; Pudło, W.; Mrowiec-Białoń, J.; Czardybon, A.; Kocurek, J.; Jarzębski, A.B. Immobilization of invertase on silica monoliths with hierarchical pore structure to obtain continuous flow enzymatic microreactors of high performance. *Microporous Mesoporous Mater.* **2013**, *170*, 75–82. [CrossRef]
33. Alvarado-Huallanco, M.B.; Maugeri Filho, F. Kinetic studies and modelling of the production of fructooligosaccharides by fructosyltransferase from *Rhodotorula* sp. *Catal. Sci. Technol.* **2011**, *1*, 1043–1050. [CrossRef]
34. Kim, M.H.; In, M.J.; Cha, H.J.; Yoo, Y.J. An empirical rate equation for the fructooligosaccharide-producing reaction catalyzed by β-fructofuranosidase. *J. Ferment. Bioeng.* **1996**, *82*, 458–463. [CrossRef]
35. Yun, J.W.; Kim, D.H.; Kim, K.W. Theoretical calculation of the sugar concentrations during enzymatic production of fructooligosaccharides. *Biotechnol. Tech.* **1996**, *10*, 871–874. [CrossRef]
36. Lee, W.C.; Chiang, C.J.; Tsai, P.Y. Kinetic modeling of fructo-oligosaccharide production catalyzed by immobilized β-fructofuranosidase. *Ind. Eng. Chem. Res.* **1999**, *38*, 2564–2570. [CrossRef]
37. Shuler, M.; Kargi, F.; DeLisa, M. *Bioprocess Engineering: Basic Concepts*; Prentice Hall: Hoboken, NJ, USA, 1992; Volume 22.
38. MathWorks (2023) Solve Stiff ODEs, MATLAB & Simulink. Available online: https://www.mathworks.com/help/matlab/math/solve-stiff-odes.html (accessed on 8 May 2023).
39. Garcia-Galan, C.; Berenguer-Murcia, Á.; Fernandez-Lafuente, R.; Rodrigues, R.C. Potential of different enzyme immobilization strategies to improve enzyme performance. *Adv. Synth. Catal.* **2011**, *353*, 2885–2904. [CrossRef]

40. Tao, Z.; Raffel, R.A.; Souid, A.K.; Goodisman, J. Kinetic studies on enzyme-catalyzed reactions: Oxidation of glucose, decomposition of hydrogen peroxide and their combination. *Biophys. J.* **2009**, *96*, 2977–2988. [CrossRef] [PubMed]
41. Gibson, Q.H.; Swoboda, B.E.P.; Massey, V. Kinetics of Action of Glucose. *J. Biol. Chem.* **1964**, *239*, 3927–3934. [CrossRef]
42. Chastang, T.; Pozzobon, V.; Taidi, B.; Courot, E.; Clément, C.; Pareau, D. Resveratrol production by grapevine cells in fed-batch bioreactor: Experiments and modelling. *Biochem. Eng. J.* **2018**, *131*, 9–16. [CrossRef]
43. Cruz, A.J.G.; Silva, A.S.; Araujo, M.L.G.C.; Giordano, R.C.; Hokka, C.O. Modelling and optimization of the cephalosporin C production bioprocess in a fed-batch bioreactor with invert sugar as substrate. *Chem. Eng. Sci.* **1999**, *54*, 3137–3142. [CrossRef]
44. Germec, M.; Turhan, I. Kinetic modeling and sensitivity analysis of inulinase production in large-scale stirred tank bioreactor with sugar beet molasses-based medium. *Biochem. Eng. J.* **2021**, *176*, 108201. [CrossRef]
45. de Moura, F.A.; Macagnan, F.T.; da Silva, L.P. Oligosaccharide production by hydrolysis of polysaccharides: A review. *Int. J. Food Sci. Technol.* **2015**, *50*, 275–281. [CrossRef]
46. Zi, Z. Sensitivity analysis approaches applied to systems biology models. *IET Syst. Biol.* **2011**, *5*, 336–346. [CrossRef]
47. Marino, S.; Hogue, I.B.; Ray, C.J.; Kirschner, D.E. A methodology for performing global uncertainty and sensitivity analysis in systems biology. *J. Theor. Biol.* **2008**, *254*, 178–196. [CrossRef]
48. Ayhan, F.; Ayhan, H.; Pişkin, E.; Tanyolac, A. Optimization of urease immobilization onto non-porous HEMA incorporated poly (EGDMA) microbeads and estimation of kinetic parameters. *Bioresour. Technol.* **2002**, *81*, 131–140. [CrossRef] [PubMed]
49. Carrara, C.R.; Rubiolo, A.C. Determination of kinetics parameters for free and immobilized β-galactosidase. *Process Biochem.* **1996**, *31*, 243–248. [CrossRef]
50. Li, C.; Lin, J.; Gao, L.; Lin, H.; Lin, J. Modeling and simulation of enzymatic gluconic acid production using immobilized enzyme and CSTR–PFTR circulation reaction system. *Biotechnol. Lett.* **2018**, *40*, 649–657. [CrossRef] [PubMed]
51. Santos-Moriano, P.; Woodley, J.M.; Plou, F.J. Continuous production of chitooligosaccharides by an immobilized enzyme in a dual-reactor system. *J. Mol. Catal. B Enzym.* **2016**, *133*, 211–217. [CrossRef]
52. IwAsAKI, K.; Inoue, M.; MATsUBARA, Y. Continuous hydrolysis of pectate by immobilized endo-polygalacturonase in a continuously stirred tank reactor. *Biosci. Biotechnol. Biochem.* **1998**, *62*, 262–267. [CrossRef]
53. Wapshott-Stehli, H.L.; Grunden, A.M. In situ H_2O_2 generation methods in the context of enzyme biocatalysis. *Enzyme Microb. Technol.* **2021**, *145*, 109744. [CrossRef]
54. Freakley, S.J.; Kochius, S.; van Marwijk, J.; Fenner, C.; Lewis, R.J.; Baldenius, K.; Marais, S.S.; Opperman, D.J.; Harrison, S.T.L.; Alcalde, M.; et al. A chemo-enzymatic oxidation cascade to activate C–H bonds with in situ generated H_2O_2. *Nat. Commun.* **2019**, *10*, 4178. [CrossRef]

Disclaimer/Publisher's Note: The statements, opinions and data contained in all publications are solely those of the individual author(s) and contributor(s) and not of MDPI and/or the editor(s). MDPI and/or the editor(s) disclaim responsibility for any injury to people or property resulting from any ideas, methods, instructions or products referred to in the content.